AD-A067 783 CALIFORNIA UNIV LIVERMORE LAWRENCE LIVERMORE LAB F/G 19/4
EXPERIMENTAL AND COMPUTER-SIMULATION STUDY OF HIGH-VELOCITY IMP--ETC(U)
DEC 78 W H GUST, D A YOUNG, J K SCUDDER W-7405-ENG-48

UNCLASSIFIED UCRL-52621 NL

| OF |
AD
A067 783

END
DATE
FILMED
6-79
DDC

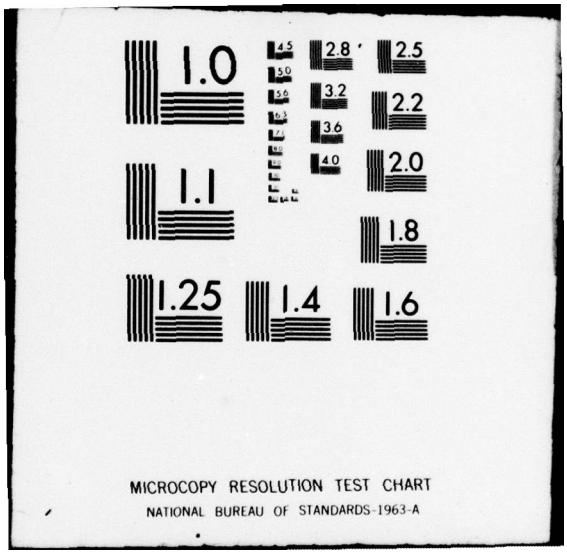
1.0
1.1
1.25
1.4
1.6
1.8
2.0
2.2
2.5
2.8
3.2
3.6
4.0
4.5
5.0
5.6
6.3
MICROCOPY RESOLUTION TEST CHART
NATIONAL BUREAU OF STANDARDS-1963-A

LEVEL II

UCRL-52621

EXPERIMENTAL AND COMPUTER-SIMULATION STUDY OF HIGH-VELOCITY IMPACT DEFORMATION IN PREHEATED MATERIALS

W. H. Gust
D. A. Young
J. K. Scudder

December 1978

20 p.

Supported by Eglin Air Force Base Project No. AFATL-8 78.

Work performed under the auspices of the U.S. Department of Energy by the UCLLL under contract number W-7405-ENG-48

LAWRENCE LIVERMORE LABORATORY
University of California/Livermore

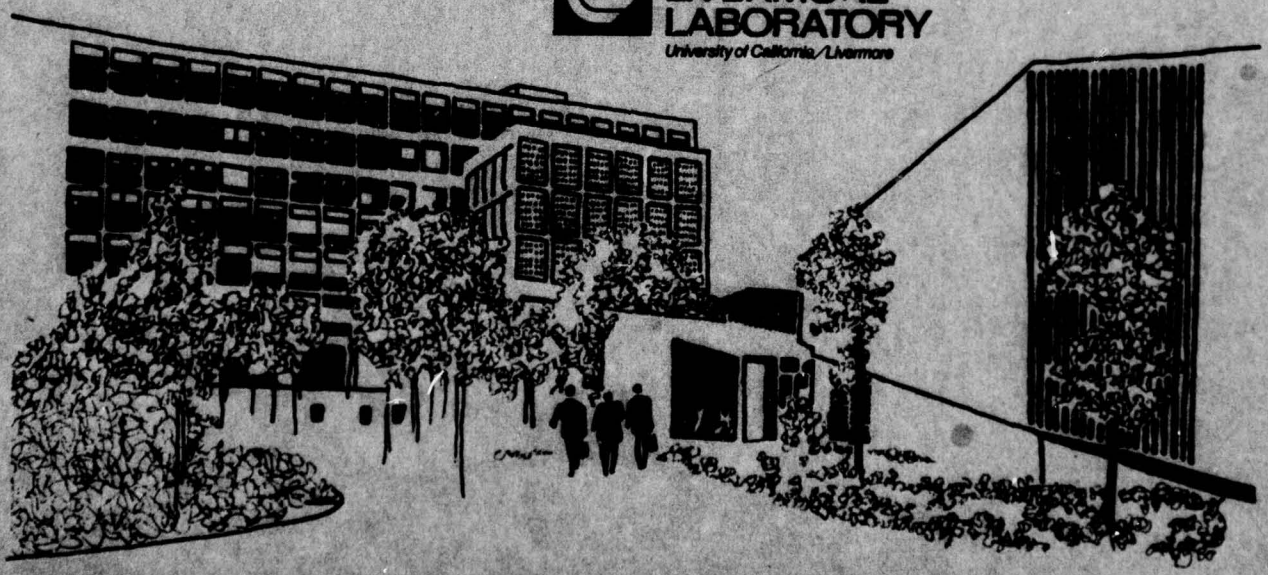

390 999

79 03 08 013

Printed in the United States of America
Available from
National Technical Information Service
U.S. Department of Commerce
5285 Port Royal Road
Springfield, VA 22161
Price: Printed Copy $; Microfiche $3.00

Page Range	Domestic Price	Page Range	Domestic Price
001–025	$ 4.00	326–350	$12.00
026–050	4.50	351–375	12.50
051–075	5.25	376–400	13.00
076–100	6.00	401–425	13.25
101–125	6.50	426–450	14.00
126–150	7.25	451–475	14.50
151–175	8.00	476–500	15.00
176–200	9.00	501–525	15.25
201–225	9.25	526–550	15.50
226–250	9.50	551–575	16.25
251–275	10.75	576–600	16.50
276–300	11.00	601–up	—[1]
301–325	11.75		

[1] Add $2.50 for each additional 100 page increment from 601 pages up.

LEVEL II

12

Distribution Category
UC-25

LAWRENCE LIVERMORE LABORATORY
University of California/Livermore, California/94550

UCRL-52621

EXPERIMENTAL AND COMPUTER-SIMULATION STUDY OF HIGH-VELOCITY IMPACT DEFORMATION IN PREHEATED MATERIALS

W. H. Gust
D. A. Young
J. K. Scudder

MS. date: December 12, 1978

CONTENTS

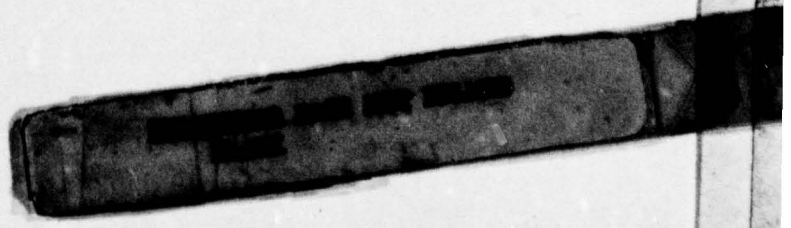

EXPERIMENTAL AND COMPUTER-SIMULATION STUDY OF HIGH-VELOCITY IMPACT DEFORMATION IN PREHEATED MATERIALS

ABSTRACT

We have developed a new "reverse gun" technique for studying high-strain-rate deformations in preheated materials. In this procedure, a rigid plate is fired at a stationary heated cylindrical rod; in contrast, the standard rifle procedure fires an unheated rod into a stationary plate. The advantage of our reverse gun method is that the rod can be preheated and the temperature monitored. We validated our technique by comparing both methods in experiments conducted at room temperature, and we obtained new deformation data for aluminum and copper rods heated to 725 K. We observed good agreement between the measured shape of the recovered rods and the shapes generated by hydrodynamic code calculations using a modified Steinberg-Guinan constitutive model and a Grüneisen equation of state.

INTRODUCTION

The U.S. Air force has expressed interest in an air-delivered penetrator that can pierce tank armor. One design developed for this type of weapon incorporates a metal-lined high explosive lens that, when detonated, ejects a slug of metal ("self-forging fragment") that forms a rod-shaped penetrator during the first moments of its flight. The penetrator retains this shape until it strikes the target.

Hydrodynamic computer codes used to design such a device and calculate its performance require input information concerning the behavior of materials at elevated temperatures and at very high strain rates ($\dot{\epsilon} > 10^4\ \text{sec}^{-1}$). The dependence of flow stress on temperature and strain rate exhibited by potential penetrator materials was therefore of particular interest, and we initiated a feasibility study at LLL to generate these experimental data. At the same time, we began a program of computer simulation in order to interpret the experimental results. We describe here these preliminary experiments and our computer simulations.

MATERIALS

The new experimental technique was initially tested on rods made from 6061-T6 aluminum and oxygen-free, high-conductivity (OFHC) copper obtained from laboratory stock. These rods received no special heat treatment prior to these tests.

The materials of primary interest were two types of electrolytic-tough-pitch (ETP) copper furnished by Eglin Air Force Base. Axially and transversely oriented rods were obtained from billets designated 114 mm (Type A) and 152 mm (Type B) ETP copper. Metallurgical details and mechanical properties are reported elsewhere.[1] The billets were machined into cylindrical rods 6 mm diam by 30 mm long that were annealed at 575 K for one hour and cooled in air.

EXPERIMENTAL METHOD

Two methods were used to study high-strain-rate plastic deformation. Data were obtained for sample rods at room temperature with a 7.62 mm rifle in the manner described by Taylor[2] and by Wilkins and Guinan[3] (Fig. 1). In this system, a moving cylindrical rod with flat ends strikes a rigid wall. Assuming that the rod decelerates as a rigid body and that plastic deformation occurs at the impact surface, we can equate the rate of decrease of rod length L with the velocity U:

$$\frac{dL}{dt} = - U \tag{1}$$

The deceleration of the rod is

$$\frac{d^2L}{dt^2} = - \frac{dU}{dt} = - \frac{Y_0}{\rho_0 L} , \tag{2}$$

where Y_0 is the flow stress (assuming an elastic-perfectly plastic model) and ρ_0 is the initial density of the rod. Combining Eqs. (1) and (2) and integrating yields

$$Y_0 = - \frac{\rho_0 U^2}{2 \ell n (L_f/L_0)} , \tag{3}$$

where L_0 and L_f are the initial and final lengths of the rod. The flow stress can thus be estimated through measurements of density, projectile velocity, and the initial and final lengths of the rod. However, because the assumptions that plastic flow occurs only at the impact surfaee and that flow stress is constant are only approximations, an accurate relationship between the flow stress and the final length of the projectile is much more complex than Eq. (3). The flow stress is generally a function of several variables and can be obtained only by comparison of experimental data with hydrodynamic code calculations.

If the velocities of the colliding bodies are interchanged so that a projectile equivalent to a rigid body strikes an unrestrained rod, Eqs. (1)-(3) are unchanged. This second method, called the "reverse gun", is illustrated in Fig. 2. The advantage of this system is that the stationary rod may be heated prior to impact which allows the relation between plastic deformation and temperature to be studied.

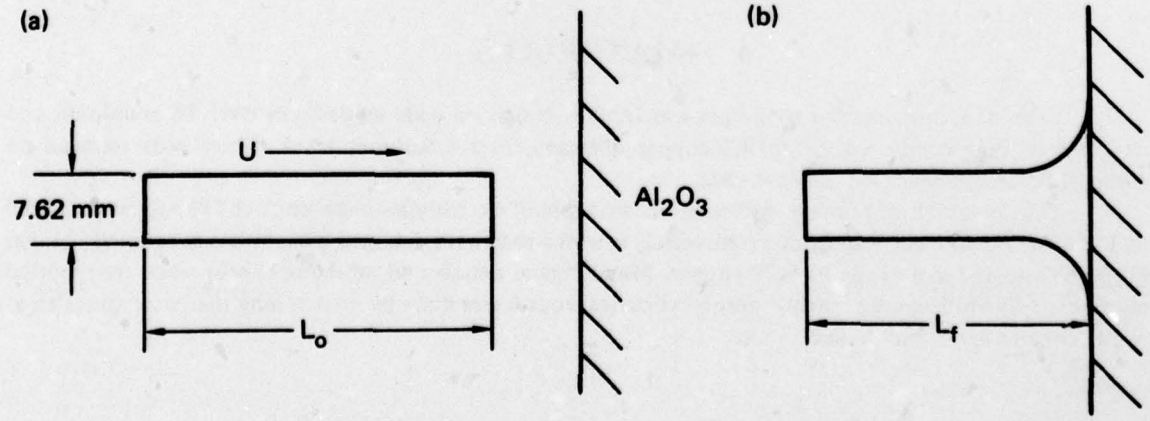

FIG. 1. Aluminum cylinder (a) before and (b) after impact on a rigid wall.

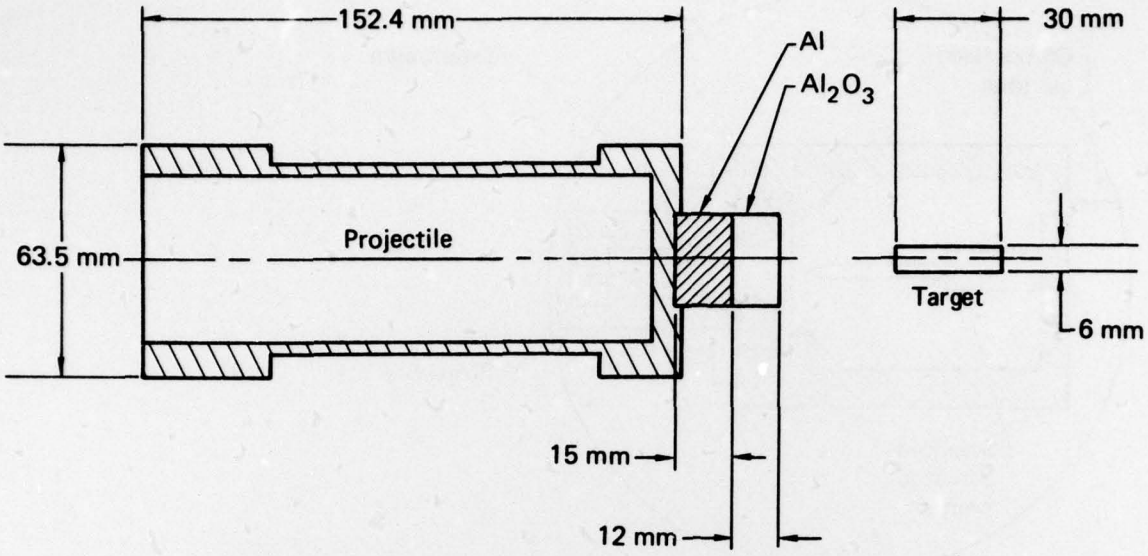

FIG. 2. Projectile and target configuration for "reverse gun" experiments.

The reverse gun experiments were conducted using a compressed-gas gun shown schematically in Fig. 3. The launch tube was 2.44 m long with a bore 63.5 mm in diameter. The impact parts of the projectile consisted of a disk of alumina (Al_2O_3) 25.0 mm in diameter and 12.0 mm thick with density 3.73 Mg/m^3. The alumina was backed by an aluminum disk 25.0 mm in diameter and 15.0 mm thick. These parts were bonded to the front face of a 63.5-mm-diam piston as shown in Fig. 2. Projectile velocity was determined using time-interval counters that measured the time between pulses generated by the short-circuiting of "whisker pins" separated by calibrated distances along the bore.

The cylindrical targets were held as shown in Fig. 4. A complete momentum exchange was assured by designing the massive projectile and target array so that complete deformation of the target rod occurred before any significant interaction between the projectile plate and the peripheral target-holding apparatus could take place; the needle-pointed support screws were notched so that they fractured easily. Variation of the plate thickness showed that target deformation was independent of this parameter.

The rods were heated to about 725 K using infrared radiation supplied by a furnace located as shown in Fig. 3. The furnace was designed so that it could be dropped from the projectile path a moment before the gun was fired. Rod temperature was monitored at the instant of impact by means of a digital readout from a thermocouple cemented to the heated rod.

The momentum trap, which allowed soft recovery of the target rods, was a 100-mm-diam by 700-mm-long cylinder of polyurethane ($\rho \cong 2$ Mg/m^3) with a 15-mm-diam by 200-mm-long hole drilled in the front end. Following impact and full target deformation, the relatively unrestrained target rod was propelled through the 15-mm-diam hole. This configuration segregated the rod from the target-holding and projectile debris. The polyurethane at the bottom of the hole decelerated the target rod without deformation.

The validity of the reverse gun data for 6061-T6 aluminum at room temperature was established by comparison with new 7.62 mm rifle shots and with rifle shot results from Ref. 3 (Fig. 5).

Some additional room temperature tests were performed on rods of OFHC copper fabricated from a single billet of LLL stock. The reverse gun data were compared with data from 6.0-mm-diam by 30-mm-long cylinders of OFHC Cu that were placed in plastic sabots and fired in a 7.62 mm rifle at an alumina disk 12.5 mm thick backed by 32 mm of steel. Figure 6 compares the results. Disagreement with data from Ref. 3 is believed to result from actual material differences, probably preshot work hardening.

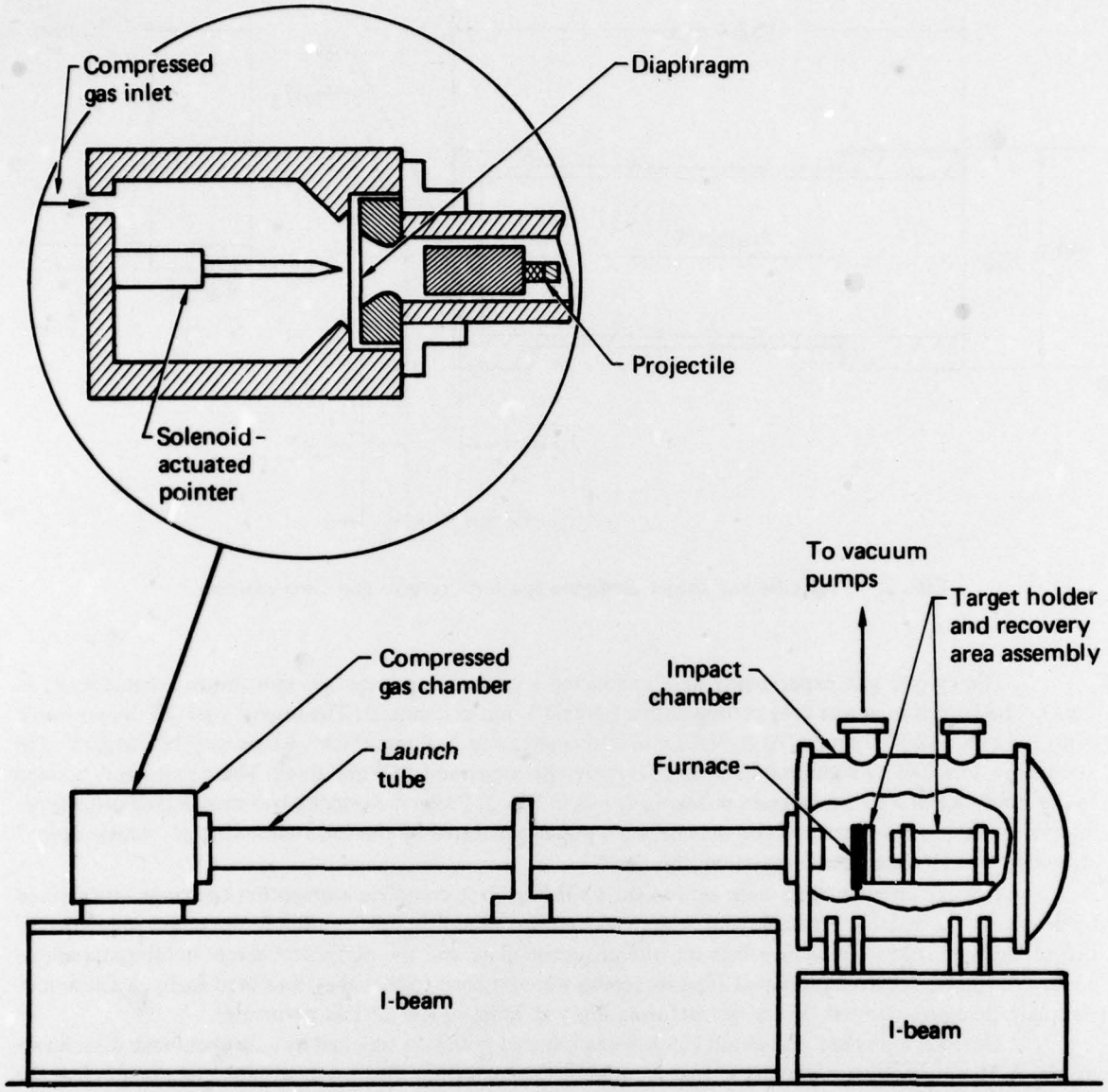

FIG. 3. Compressed-gas gun and experimental chamber assemblies used in dynamic flow stress measurements at elevated temperatures.

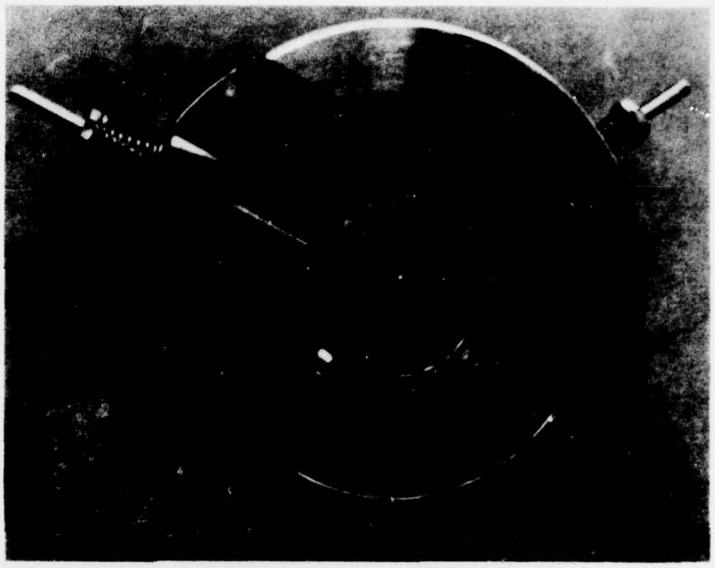

FIG. 4. Target-rod holding apparatus. The rod is supported by needle-pointed screws. The entire support system was spring-loaded to allow for thermal expansion.

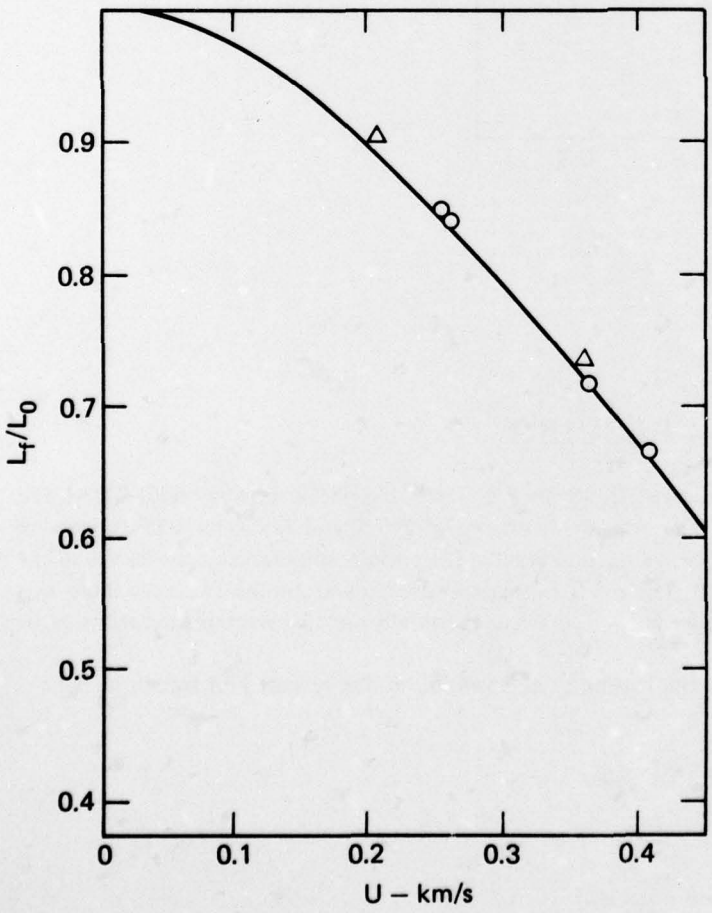

FIG. 5. Comparison of reverse-gun data (triangles) with 7.62 mm rifle data performed by us (circles) and from Ref. 3 (smooth curve) for room-temperature 6061-T6 aluminum.

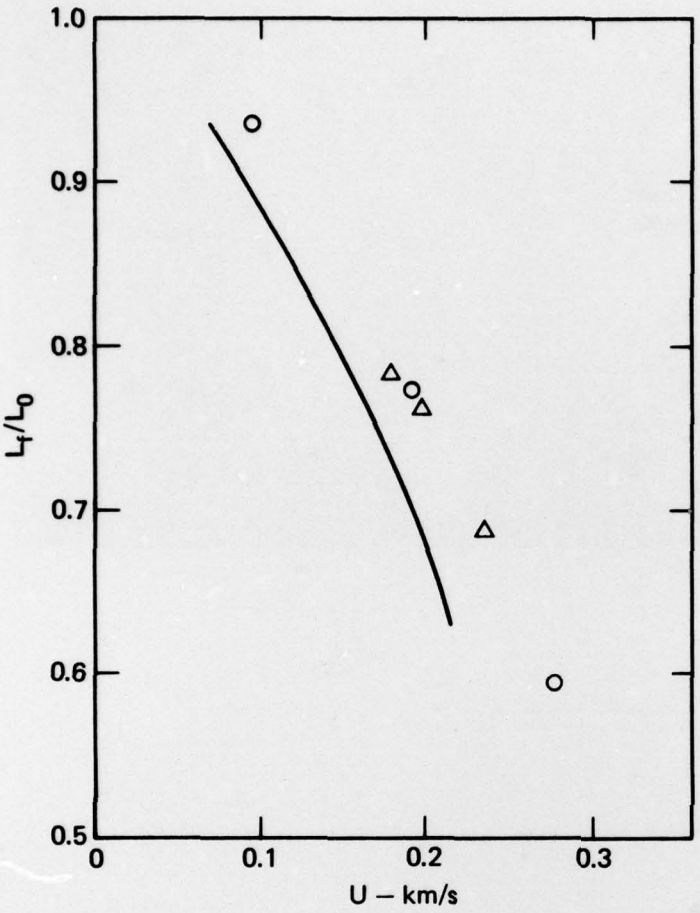

FIG. 6. Comparison of reverse-gun data (triangles) with 7.62 mm rifle data performed by us (circles) and from Ref. 3 (smooth curve) for room-temperature OFHC copper. The discrepancy between our data and those of Ref. 3 represent a significant difference in material preparation.

RESULTS

The experimental data are summarized in Tables 1-4. The cross-check data for 6061-T6 Al and OFHC Cu are displayed in Figs. 5 and 6. The plots for isotherms at 295 K and 725 K for ETP copper are shown in Fig. 7 and constitute the primary experimental results; the strong temperature dependence of the length ratio for ETP copper is clearly evident. The 295 K isotherm also demonstrates that, as far as these tests are concerned, there is no significant difference in L_f/L_0 between the axially and transversely oriented rods, or between the type A and type B materials.

These results clearly demonstrate the feasibility and validity of the reverse gun technique.

TABLE 1. Data summary for ETP copper (T = 295 K).

Shot number	Type Cu[a]	Initial density (ρ_0), Mg/m^3	Projectile velocity (U), km/s		Final length/ Initial length (L_f/L_0)
			Pins	Optics	
23	A-a	8.907	0.148	b	0.806
24	A-a	8.921	0.181	b	0.675
25	A-a	8.928	0.316	0.307	0.418
26	A-a	8.919	0.277	0.258	0.492
27	A-a	8.935	0.357	0.340	0.332
28	A-a	8.928	0.367	0.354	0.325
29	A-t	8.918	0.311	0.320	0.373
30	B-a	8.916	0.332	0.321	0.383
31	B-a	8.918	0.225	0.213	0.597
32	B-a	8.911	0.109	b	0.812
33	B-a	8.904	0.126	b	0.777
34	B-a	8.902	b	0.394	0.280
35	B-a	8.911	0.349	0.352	0.333

[a]A = 114-mm billet, B = 152-mm billet, a = rod cut axially from billet, t = rod cut transversely from billet.
[b]No record.

TABLE 2. Data summary for preheated ETP copper.

Shot number	Type Cu[a]	Initial density (ρ_0), Mg/m^3	Temperature (T), K	Projectile velocity (U), km/s	Final length/ Initial length (L_f/L_0)	Comments
52	A-a	8.930	718	0.188	0.555	
53	A-a	8.928	765	0.237	0.391	Large peripheral cracks
55	A-a	8.928	703	0.145	0.690	
56	A-a	8.929	721	0.210	0.507	Bent off-axis during recovery
57	A-a	8.927	724	0.206	0.529	Slight peripheral cracking
58	A-t	8.913	733	0.19	0.574	U obtained from loading curve
60	A-t	8.929	717	0.142	0.718	
61	A-t	8.947	727	0.211	0.516	
62	A-t	8.935	721	0.115	0.769	
63	A-t	8.937	718	0.0487	0.993	
64	A-t	8.929	727	0.191	0.562	

[a]A = 114 mm billet, a = rod cut axially from billet, t = rod cut transversely from billet.

TABLE 3. Data summary for OFHC copper (T = 295 K).

Shot number	Initial density (ρ_0), Mg/m^3	Projectile velocity (U), km/s	Final length/ Initial length (L_f/L_0)	Comments
38	8.930	0.177	0.784	Reverse gun data
43	8.907	0.194	0.764	Reverse gun data
45	8.912	0.233	0.688	Reverse gun data
48	8.912	0.0895	0.933	7.62 mm rifle data
50	8.907	0.189	0.774	7.62 mm rifle data
51	8.930	0.276	0.596	7.62 mm rifle data

TABLE 4. Data summary for 6061-T6 aluminum.

Shot number	Initial density (ρ_0), Mg/m^3	Initial temperature (T), K	Projectile velocity (U), km/s	Final length/ Initial length (L_f/L_0)	Comments
18	2.685	295	0.252	0.848	7.62 mm rifle data
19	2.691	295	0.257	0.841	7.62 mm rifle data
20	2.687	295	0.361	0.717	7.62 mm rifle data
21	2.651	295	0.406	0.663	7.62 mm rifle data
39	2.708	295	0.20	0.903	Reverse gun data
40	2.708	295	0.358	0.735	Reverse gun data
41	2.710	635	0.194	0.770	Reverse gun data
42	2.707	655	0.354	0.397	Reverse gun data

COMPUTER CALCULATIONS

To conduct hydrodynamic computer code simulations, we need a complete constitutive model that incorporates a pressure equation of state (EOS) and expressions for the shear modulus G and flow stress Y.

Since the material in our experiments is not heated above the melting point, we are interested in an EOS for the solid phase only. Specifically, we choose the Mie-Grüneisen model,

$$P(V,T) - P(V,0) = \frac{\gamma(V)}{V} [E(V,T) - E(V,0)] \ , \tag{4}$$

where P is the pressure, V is the volume, E is the internal energy, and γ is the Grüneisen parameter. Since the zero Kelvin curve P(V,0) has not been measured, we must compute it from another reference curve, namely, the Hugoniot. Thus

$$P_H(V) - P(V,0) = \frac{\gamma(V)}{V} [E_H(V) - E(V,0)] \ , \tag{5}$$

where

$$E_H(V) = \frac{1}{2} P_H(V) (V_0 - V)$$

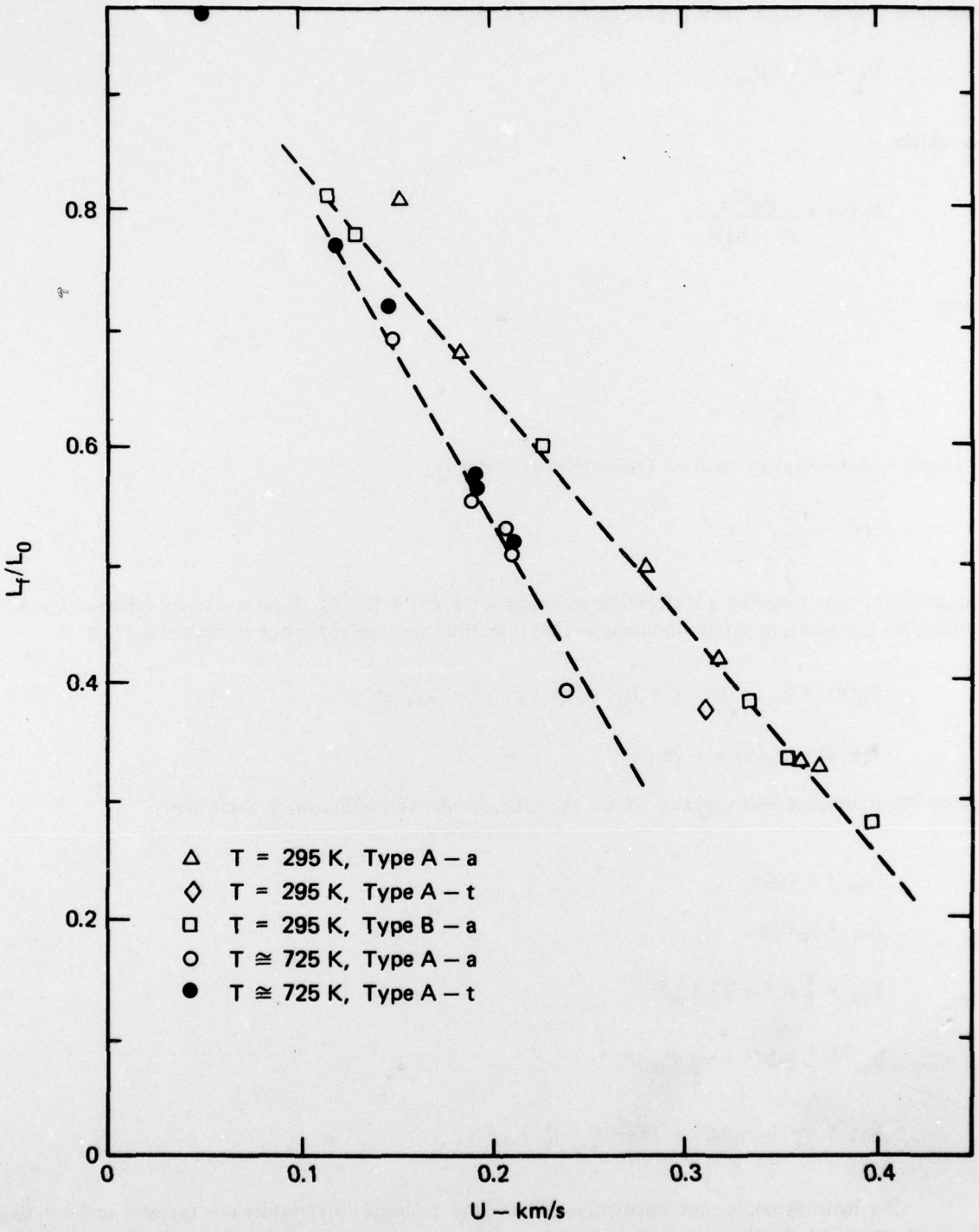

FIG. 7. Experimental ETP copper isotherms for 295 K and approximately 725 K showing linear behavior over the measured velocity range. These curves indicate that, for the same impact velocity, a heated rod is significantly shorter after impact than a rod at room temperature. The greater deformation is attributed to decreased flow stress at the higher temperature.

Assuming a linear shock velocity-particle velocity relation

$$U_S = C + SU_p ,$$

we obtain

$$P_H(V) = \frac{\rho_0 C^2 x}{(1 - Sx)^2} ,$$

where

$$x = 1 - \frac{V}{V_0} .$$

A simple and moderately accurate Grüneisen parameter is

$$\gamma(V) = \frac{\gamma_0 V}{V_0} .$$

Equation (5) now becomes a differential equation for $E_0(V) = E(V,0)$. A power series expansion in x is suitable for E_0, since only small compressions (less than 10%) are expected in our experiments. Thus

$$E_0(V) = E_{00} + E_{01}\, x + E_{02}\, x^2 + E_{03}\, x^3 + E_{04}\, x^4 ,$$

$$P(V, 0) = P_0(V) = - \partial E_0 / \partial V .$$

Assuming a constant heat capacity 3R for the solid, we derive the following coefficients:

$$E_{00} = - 900R ,$$

$$E_{01} = \gamma_0 E_{00} ,$$

$$E_{02} = \frac{1}{2} (C^2 + \gamma_0^2\, E_{00}) ,$$

$$E_{03} = \frac{1}{6} (4SC^2 + \gamma_0^3\, E_{00}) ,$$

$$E_{04} = \frac{1}{24} (-2\gamma_0 SC^2 + 18S^2C^2 + \gamma_0^4\, E_{00}) .$$

For hydrodynamic code calculations, we use the independent variables $\mu = (\rho/\rho_0)-1$ and $e = E\rho_0$. We need expressions for the pressure $P(\mu,e)$ and the temperature $T(\mu,e)$. For the compressions found in the experiments, it was sufficient to take the pressure expansion to μ^3 and the temperature expansion to μ^4. Thus

$$P(\mu, e) = P_0(\mu) + \frac{\gamma(V)}{V\rho_0}\,[e - e_0(\mu)]$$

$$= \rho_0 C^2 \mu + \rho_0 C^2 \left[\left(1 - \frac{\gamma_0}{2}\right) + 2(S - 1)\right] \mu^2$$

$$+ \rho_0 C^2 \left[2\left(1 - \frac{\gamma_0}{2}\right)(S - 1) + 3(S - 1)^2\right]\mu^3 + \gamma_0 e \ , \qquad (6)$$

and

$$T(\mu, e) = \left[e/\rho_0 - E_{00} - E_{01}\mu - (-E_{01} + E_{02})\mu^2 - (E_{01} - 2E_{02} + E_{03})\mu^3 \right.$$

$$\left. - (-E_{01} + 3E_{02} - 3E_{03} + E_{04})\mu^4 \right] /3R \ . \qquad (7)$$

We now consider models of the shear modulus (G) and flow stress (Y). First, we need an expression for the melting temperature as a function of volume, because G and Y will drop abruptly to zero at the melting point. We use the Lindemann melting law,[4] which works well for metals like Al and Cu:

$$T_m(x) = T_{m0} \exp(2\gamma_0 x)\,(1 - x)^{2/3} \ .$$

The flow stress Y is a scalar quantity and must be compared with a scalar invariant of the stress tensor. Specifically, the von Mises yield criterion is used:

$$(\sigma_1 - \sigma_2)^2 + (\sigma_2 - \sigma_3)^2 + (\sigma_3 - \sigma_1)^2 = 2Y^2 \ ,$$

where the values of σ are the principal stresses. If the stress invariant is less than $2Y^2$, the motion is elastic; if it is greater, then the motion is plastic.

For G and Y, we use the Steinberg-Guinan (SG) model[5]:

for $T < T_m$,

$$G = G_0 \left[1 + b\,\frac{P}{\eta^{1/3}} + h\,(T - 300)\right],$$

$$Y = Y_0 \left[1 + \beta(\bar{\varepsilon}^p + \bar{\varepsilon}_i^p)\right]^n \left[1 + b\,\frac{P}{\eta^{1/3}} + h(T - 300)\right], \qquad (8)$$

where

$$Y_0 \left[1 + \beta(\bar{\varepsilon}^p + \bar{\varepsilon}_i^p)\right]^n \le Y_{max} \ ;$$

for $T > T_m$,

$$G = 0 \ ,$$

$$Y = 0 \ . \qquad (9)$$

In this case,

$$\eta = \frac{\rho}{\rho_0} \ ,$$

$$\bar{\epsilon}^p = \text{equivalent plastic strain} = \int \dot{\bar{\epsilon}}^p \, dt \ ,$$

$$\dot{\bar{\epsilon}}^p = \frac{\sqrt{2}}{3} \left[\left(\dot{\epsilon}_1^p - \dot{\epsilon}_2^p\right)^2 + \left(\dot{\epsilon}_2^p - \dot{\epsilon}_3^p\right)^2 + \left(\dot{\epsilon}_3^p - \dot{\epsilon}_1^p\right)^2 \right]^{1/2} \ ,$$

and $\bar{\epsilon}_i^p$ is the initial equivalent plastic strain. The constants b, h, β, n, G_0, Y_0, and Y_{max} are tabulated for each material; the values of Y_0 in Eqs. (3) and (8) are not the same, however. No explicit strain-rate dependence has been assumed for Y in these calculations.

The SG model predicts that the shear modulus increases with pressure and decreases with temperature, dropping discontinuously to zero at $T \geq T_m$. The flow stress model uses the same coefficients b and h for pressure and temperature dependence since the behavior of Y is expected to be very similar to that of G. In addition, a work-hardening function dependent on the coefficients β and n allows Y to increase smoothly with plastic strain. The effect of work hardening is given an upper limit Y_{max}.

For simulation of impact, we used HEMP, a two-dimensional Lagrangian hydrodynamic code.[6] At the end of each time step, the state of strain and the energy in each zone were calculated. These data were used to compute T and P and then Y and G for use in the subsequent step.

Our objective was to compare the hydrodynamic calculations with experimental data over a range of impact velocities and initial temperatures and to determine how well the SG constitutive model reproduces the final length and shape of the rods. We considered for this comparison 6061-T6 aluminum and ETP copper; a complete listing of coefficients for these two metals is given in Table 5. These calculations are expensive in terms of computer time, and therefore we ran only a few comparisons with experiments.

Each calculation was set up initially as an axisymmetric rod with initial values of ρ, e, and velocity U. The front face of the rod was in contact with a rigid boundary that was perpendicular to the rod axis. The initial configuration with 7 × 26 zones is shown in Fig. 8. As the rod struck the boundary, the equivalent stress

TABLE 5. Constitutive model and EOS parameters for aluminum and copper.

Parameter	Al (6061-T6)	Cu (ETP)
R (J/kg-K)	308.2	130.8
ρ_0 (Mg/m^3)	2.705	8.930
C (km/s)	5.33	3.94
S	1.338	1.489
γ_0	2.18	1.99
b	8.0	2.8
h	-6.2×10^{-4}[a]	-3.8×10^{-4}[a]
	-1.5×10^{-3}[b]	-9.2×10^{-4}[b]
G_0 (GPa)	27.6	47.7
β	125	36
n	0.10	0.45
Y_0 (GPa)	0.29[a]	0.12[a]
	0.32[b]	0.125[b]
Y_{max} (GPa)	0.68	0.64
T_{m0} (K)	1220	1790

[a]SG tabulated value.
[b]Best fit to data.

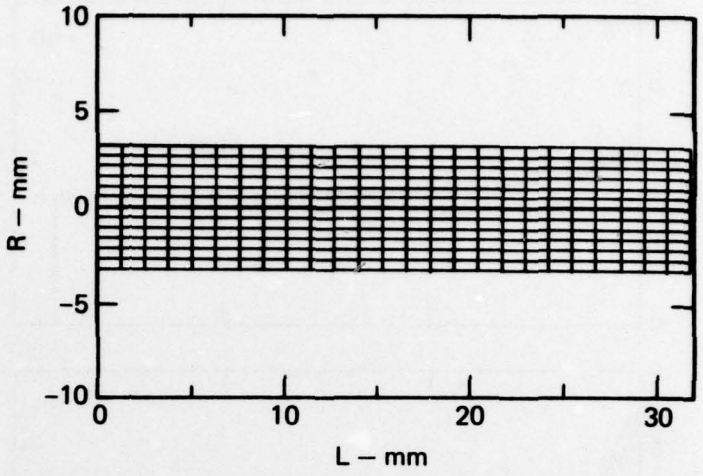

FIG. 8. Initial configuration of the rod in HEMP calculations. The rod is a 6.4-mm-diam by 31.77-mm-long cylinder divided into 7 radial and 26 axial zones. The rigid wall is at the left boundary.

exceeded Y in the front zones and these zones deformed plastically in the radial direction. As stress waves moved back and forth along the rod, the forward momentum of the rod diminished gradually, and a wave of plastic deformation moved away from the impact surface. At the same time, heating and work hardening occurred. Plastic deformation eventually ceased and the rod underwent elastic oscillations of small amplitude. This process for Al and Cu was completed in 40 to 100 μsec, depending on the initial conditions.

Our approach to fitting the computer simulation to the experimental data evolved through a series of calculations. We considered Y_0 and h to be adjustable parameters. Y_0 was determined by comparing simulations with experiments at low velocity on room temperature rods in the spirit of Eqs. (1)-(3). Under these conditions, the effects of heating due to impact are negligible and the term that contains h is therefore unimportant.

The curve of L_f/L_0 vs U for aluminum at room temperature was approximated reasonably well by the SG model if $Y_0 = 0.32$ GPa (rather than the 0.29 GPa value reported in Ref. 5). For the shots with preheated rods, we used the EOS to determine the values of the independent variables μ and e corresponding to P = 0 and the desired value of T. It is significant that the temperature coefficient $h = -6.2 \times 10^{-4}$, given in Ref. 5, is too small to simulate the preheated shots and predicts a value of L_f that is too large. Several trials demonstrated that a better value is $h = -1.5 \times 10^{-3}$. Using these new parameter values, our calculation fits the experimental room temperature curve adequately, and it also fits shot 41, with T = 615 K, rather accurately. An attempt to fit shot 42 failed because the numerous rezones required by the extreme flattening of the front zones impaired the accuracy of the calculation.

To this point, we have only discussed our attempts to predict the final length of the rod. A sensitive test of the constitutive model, and especially of the effect of work-hardening on flow stress, is the shape of the rod after impact. Figure 9 compares the shape of the three aluminum simulations and experiments.

A series of HEMP runs in which U = 0.189 km/s and Y_0 was varied showed that the room temperature copper data of all types was covered by the range $0.12 \leq Y_0 \leq 0.25$ GPa. This extent of this range of values appears to reflect the different work hardening experienced by the various types of copper prior to our experiments.

We were primarily interested in fitting the room temperature and preheated ETP data and found that a value $Y_0 = 0.125$ GPa provided an adequate fit of the room temperature ETP curve. An attempt to fit shot 52, which was preheated to 718 K and had an impact velocity of 0.188 km/s, once again showed that the SG temperature coefficient was too small. Changing the value of h from -3.8×10^{-4} to -9.2×10^{-4} yielded adequate agreement with the measured final length.

Two additional long runs (to 100 μs) were performed to check the calculations against shots 26 (room temperature) and 61 (preheated). Fracture at the rim of the impact surface in shot 26 prevented accurate comparison of the measured shape with the calculations for this surface. Comparisons of measured and calculated shapes for shots 26, 52, and 61 are shown in Fig. 10.

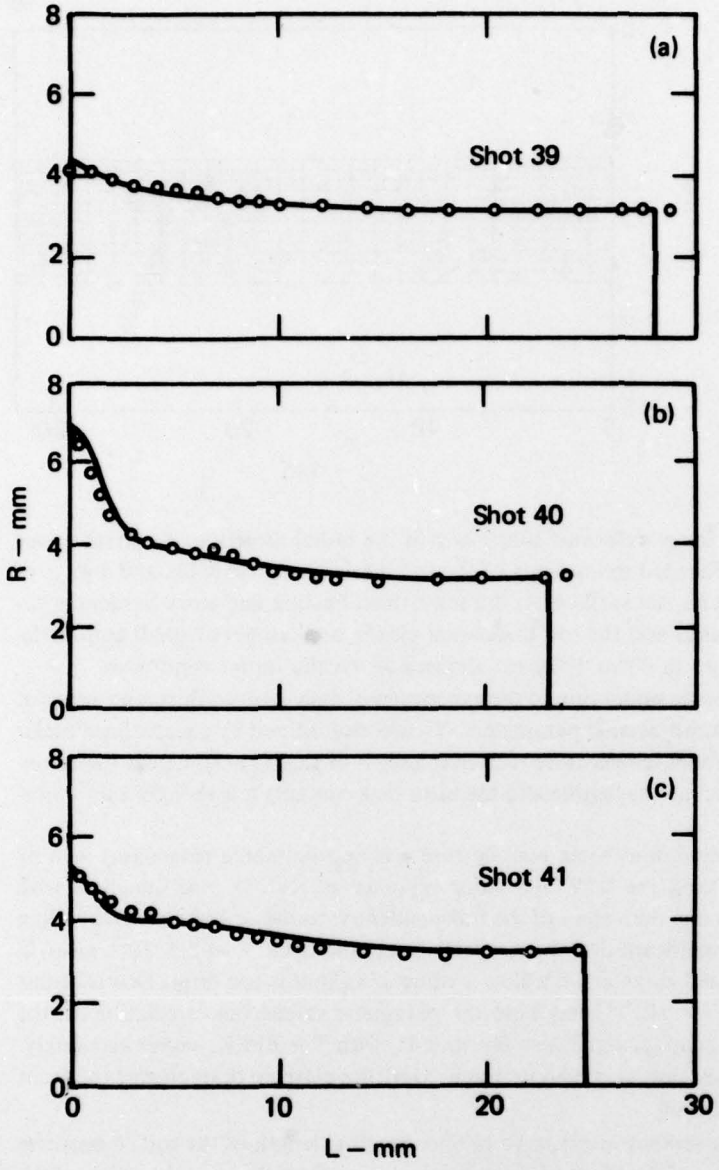

FIG. 9. Comparison of HEMP calculations (smooth curves) with experimental measurements (circles) of the profiles of deformed aluminum rods from shots 39, 40, and 41. The R (radial) and L (axial) axes are not to scale. (a) U = 0.20 km/s, T = 295 K; (b) U = 0.358 km/s, T = 295 K; (c) U = 0.194 km/s, T = 635 K.

The agreement between experiment and calculation is good, considering that only two of the parameters in the SG model were varied. The parameters in the work-hardening term as given in Ref. 5 thus appear to be well chosen. Work-hardening effects are responsible for the inflection observed in the profiles of the deformed rods. Because the experiments appear to have a consistently steeper profile in the inflection region than the calculations, a better fit of the calculated curves to experiment might be obtained by adjusting the work-hardening parameters n and β slightly.

The SG model assumes that Y_0 is a fixed property of the material and that any previous work hardening is included in the initial plastic strain $\bar{\varepsilon}_i^p$. We have instead set $\bar{\varepsilon}_i^p = 0$ and have assumed that materials

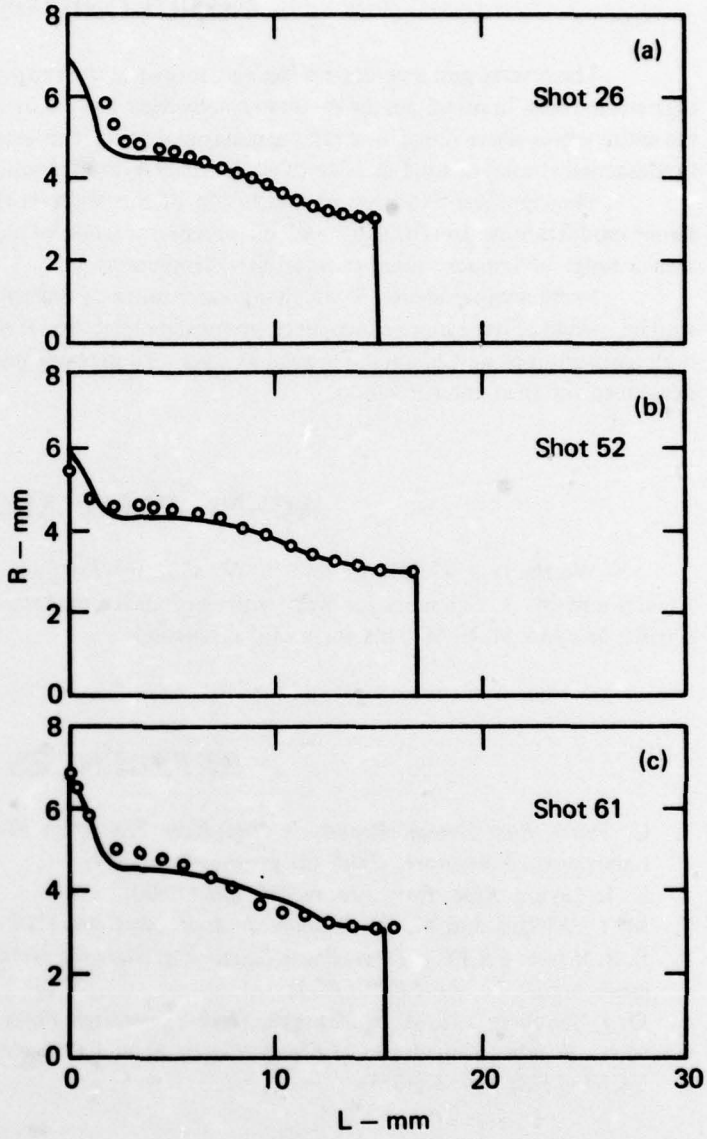

FIG. 10. Comparison of HEMP calculations (smooth curves) with experimental measurements (circles) of the profiles of deformed ETP copper rods from shots 26, 52, and 61. The R (radial) and L (axial) axes are not to scale. (a) U = 0.277 km/s, T = 295 K; (b) U = 0.188 km/s, T = 718 K; (c) U = 0.211 km/s, T = 727 K.

with different work-hardening histories have different Y_0 values. In either case, Y_0 or $\bar{\epsilon}_i^R$ are treated as adjustable parameters.

In these calculations we changed h, the coefficient of temperature dependence in the shear modulus and flow stress, in order to fit the final length of the preheated rods. This procedure was not quite correct, since the temperature dependence of the shear modulus had been measured and it should have remained at the measured value. In future calculations, the temperature coefficients of G and Y should be varied independently.

CONCLUSIONS

The reverse gun technique effectively measures the temperature dependence of material properties at high strain rates. In principle, the material can be heated up to its melting point and measurements taken over the entire temperature range in which the material is solid. This measurement capability should prove useful in fundamental studies of solid mechanics as well as in hydrodynamic code simulation of self-forging fragments.

The significant theoretical conclusion of this work is that the SG constitutive model, with some minor modifications, can furnish an adequate representation of plastic deformations in aluminum and copper over a range of impact velocities and initial temperatures.

Further experiments, in which a greater range of materials, impact velocities, and temperatures are studied, would allow a more exact check on the dependability of the SG model. At high impact velocities and high temperatures, new phenomena such as fracture and shock melting could be studied and models could be developed for their interpretation.

ACKNOWLEDGMENTS

We thank J. G. Moore and V. W. Morasch for their assistance with the gun experiments, S. J. French and M. A. Schnabel for help with code development and execution, and D. J. Steinberg, D. M. Norris, Jr., and M. L. Wilkins for useful discussions.

REFERENCES

1. C. Tatro, *First Annual Report on High-Rate Testing at Elevated Temperatures,* Lawrence Livermore Laboratory, Livermore, Calif. (in preparation, 1979).
2. G. I. Taylor, *Proc. Roy. Soc.* A **194**, 289 (1948).
3. M. L. Wilkins and M. W. Guinan, *J. Appl. Phys.* **44**, 1200 (1973).
4. E. B. Royce, *GRAY, a Three-Phase Equation of State for Metals,* Lawrence Livermore Laboratory, Livermore, Calif., UCRL-51121 (1971).
5. D. J. Steinberg and M. W. Guinan, *High Temp-High Press.* (in press, 1979).
6. M. L. Wilkins, *Calculation of Elastic-Plastic Flow.* Lawrence Livermore Laboratory, Livermore, Calif., UCRL-7322, Rev. I (1969).

KMG/bm